

# The diffuse interstellar bands at 5797, 6379 and 6613 Å

## Ionization properties of the carriers<sup>\*</sup>

P. Sonnentrucker<sup>1,2</sup>, J. Cami<sup>3,4</sup>, P. Ehrenfreund<sup>5,6</sup>, and B.H. Foing<sup>1,6</sup>

<sup>1</sup> Solar System Division, ESA Space Science Department, ESTEC/SO, PB 299, 2200 AG Noordwijk, The Netherlands

<sup>2</sup> Observatoire de Strasbourg, 11 rue de l'Université, F-67000 Strasbourg, France

<sup>3</sup> SRON Groningen, P.O. Box 800, 9700 AV Groningen, The Netherlands

<sup>4</sup> Astronomical Inst. "Anton Pannekoek", Univ. of Amsterdam, Kruislaan 403, 1098 SJ Amsterdam, The Netherlands

<sup>5</sup> Leiden Observatory, P.O. Box 9513, 2300 RA Leiden, The Netherlands

<sup>6</sup> Institut d'Astrophysique Spatiale, CNRS, Bat 121, Campus d'Orsay, F-91405 Orsay, France

Received 5 May 1997 / Accepted 11 July 1997

**Abstract.** We present a study of the behaviour and ionization properties of three narrow Diffuse Interstellar Bands (DIBs) at  $\lambda\lambda 5797$ , 6379 and 6613 Å. In all three DIBs substructures have recently been detected, indicating large gaseous molecular carriers. Studying DIBs in regions with drastically different physical properties in terms of UV flux and density enables us to monitor the behaviour of the carriers and hence to constrain their nature. We observed these three DIBs along 40 different lines-of-sight (35 program stars and 5 standard stars) consisting of HII regions, dark clouds, molecular clouds and reflection nebulae. The DIB variations at low reddening are explained by a new model of photoionization equilibrium of the DIB carriers. This model takes into account the penetration depth of UV ionizing photons throughout the cloud. The slope of the variation of DIB strength as a function of reddening thus allows us to estimate the effective ionization potentials of the carriers. Following this new analysis, the carriers of the  $\lambda 5797$  and  $\lambda 6613$  Å DIBs would have ionization potentials above 10 eV, reminiscent of large PAHs or fullerenes which have a single positive charge. The estimated ionization potential (7–9 eV) of the  $\lambda 6379$  Å DIB seems to indicate a large neutral carrier.

**Key words:** ISM: molecules – ISM: molecular clouds, HII regions – molecular processes – line: identification

### 1. Introduction

More than 150 unidentified Diffuse Interstellar Bands (DIBs) are seen in absorption in the visible spectrum towards reddened

---

*Send offprint requests to:* P. Sonnentrucker

<sup>\*</sup> Based on observations with OHP 1.93m Telescope and Elalieg spectrograph.

stars (Herbig 1995). They have been detected in different regions of the interstellar medium indicating an ubiquitous presence of their carriers in space. Several assumptions ranging from solid state to gas phase origin were made concerning the nature of these carriers. Though recent studies point strongly towards a gas phase molecular origin for many DIBs, the carrier molecules are not yet identified (see Herbig 1995 for a review).

Laboratory studies on Polycyclic Aromatic Hydrocarbons (PAHs) show that PAH ions may reproduce the diffuse band behaviour (Salama et al. 1996). Two diffuse bands were detected in the near-infrared at  $\lambda\lambda 9577$  Å and 9632 Å, which are consistent with laboratory spectroscopic data on  $C_{60}^+$  (Foing & Ehrenfreund 1994, 1997). An assembly of observed diffuse bands into families has been discussed by Krelowski & Walker (1987) using ratios of well-defined DIBs as indicators. A recent correlation study of 44 DIBs towards single cloud stars shows that only a few DIBs correlate rather well (Cami et al. 1997).

High resolution spectroscopy showed that some DIBs have double or triple-peak substructures (Sarre et al. 1995, Ehrenfreund & Foing 1995, 1996, Krelowski & Schmidt 1997). The comparison of rotational contour calculations and astronomical DIB profiles suggest that the  $\lambda 5797$  Å and  $\lambda 6379$  Å may originate in large gas phase molecules with 50 C atoms. The  $\lambda 6613$  Å DIB is consistent with molecules of 40 C atoms, assuming the PAH analogy, but could also originate from a  $C_{60}$  fullerene compound, 12-18 C chains or C-rings (Ehrenfreund & Foing 1996). Recent modelling of the  $\lambda 6613$  Å DIB led Kerr et al. (1996) to the conclusion that rings containing 14–30 C could reproduce the observed substructures of the  $\lambda 6613$  Å DIB.

Previous surveys showed that DIBs have different behaviour linked to the changes of physical and chemical properties of interstellar clouds (Snow & Cohen 1974, Adamson et al. 1991, Jenniskens et al. 1994, Krelowski et al. 1996). Many DIBs are weak in Photon-Dominated Regions (PDR) as well as in dense molecular clouds in comparison to their average inter-

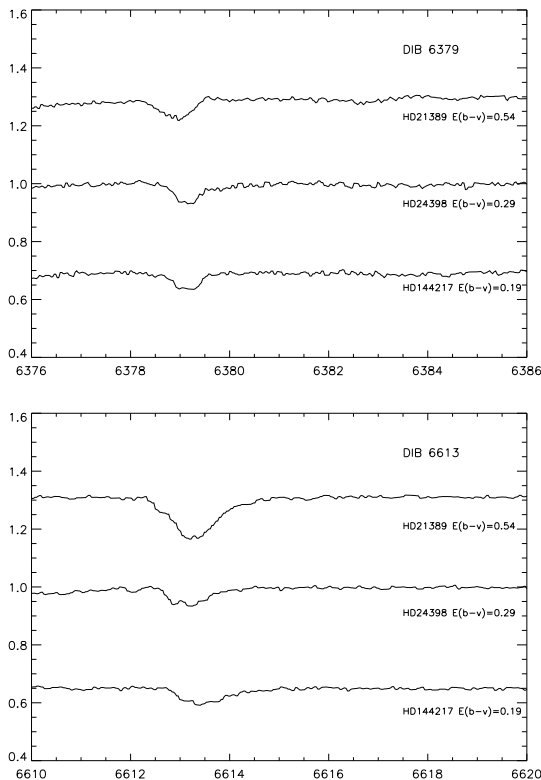


**Fig. 1.** Spectra showing the  $\lambda\lambda 6379$  and  $6613$  Å DIBs in the diffuse medium star HD21389, the Taurus star HD24398 and the Sco-Oph star HD144217, with  $E_{(B-V)}$  equal to 0.54, 0.29 and 0.19 respectively.

stellar medium strength. They also seem to have a rather puzzling behaviour in reflection nebulae, being either enhanced or weakened in an unsystematic way (see e.g. Snow et al. 1995). A correlation study of the  $\lambda\lambda 5780$  and  $5797$  Å DIBs with NaI, KI, Cl, HI and  $H_2$  led Herbig (1993) to the conclusion that these two DIBs were likely to be produced by neutral gaseous carriers with an ionization/dissociation threshold somewhat higher than 5.1 eV.

This paper reports the results on the study of the environmental behaviour of the  $\lambda\lambda 5797$ ,  $6379$  and  $6613$  Å DIBs in 40 different lines-of-sight and discusses their implications for the nature of the carrier molecules.

## 2. Observations

### 2.1. Data acquisition

By using the “*ELODIE*” spectrograph, observations were performed at the 1.93 m telescope at the *Observatoire de Haute Provence* (OHP) in July and November 1995. The “*Elodie*” spectrograph covers the wavelength range  $\lambda 3906$ – $6811$  Å with a spectral resolving power of 42,000. Exposure times were estimated in order to obtain a S/N of  $\sim 300$ . Fig. 1 gives an example of spectra obtained during these campaigns. HD21389 is representative for diffuse medium conditions and has an  $E_{(B-V)}$  of 0.54. HD24398 is a star located in a dense region

of the Taurus molecular cloud. From the spectra we can see the environment dependence of the  $\lambda\lambda 6379$  and  $6613$  Å DIBs.

### 2.2. Equivalent widths

Stellar and atmospheric contamination were corrected if necessary by dividing the stellar spectra at similar airmass by a standard star of possibly same fundamental parameters (such as spectral type). All reference stars used have negligible reddening. The equivalent width ( $W$ ) was measured after corrections were applied, and then normalized to unit reddening, as summarized in Table 1.

## 3. Results and discussion

### 3.1. Environmental behaviour

The linear Pearson correlation coefficients were calculated for the  $\lambda\lambda 5797$ ,  $6379$  and  $6613$  Å DIBs using the normalized equivalent width measured towards all stars. The  $\lambda 5797$  Å DIB was used as reference. The calculation shows that  $\lambda 6379$  Å correlates with  $\lambda 5797$  Å with a factor of 0.80. As far as  $\lambda 6613$  and  $\lambda 5797$  Å are concerned, the correlation coefficient is equal to 0.69. They slightly differ from Cami et al. (1997) recent mutual correlation calculations towards single cloud lines-of-sight (correlation coefficients of 0.85 for  $\lambda\lambda 5797$  and  $6379$  Å and 0.78 for  $\lambda\lambda 5797$  and  $6613$  Å, respectively). This is due to the use of a different target sample but, nevertheless, both results show the same trend: these three DIBs have a similar behaviour i.e. they have the tendency to be all enhanced or weakened together. They appear to be weakened the same efficient way in all lines-of-sight in Orion except for HD36861, even though studies on rotational contours indicate that the three DIBs at  $\lambda\lambda 5797$ ,  $6379$  and  $6613$  Å originate from carriers with close but different number of carbon atoms (at least for  $\lambda 5797$  and  $\lambda 6613$  Å DIBs, see Ehrenfreund and Foing 1996). Towards HD36861, the  $\lambda 5797$  Å DIB is much stronger than the two other DIBs. A further study of this line-of-sight may allow to find out if this peculiar behaviour is due to a systematic error or really witnesses differences in the properties of the carrier molecules in Orion.

In Fig. 2, the decimal logarithm of the normalized equivalent width  $W/E_{(B-V)}$ , measured for the three DIBs towards the Orion and Taurus-Perseus targets, is plotted against reddening,  $E_{(B-V)}$ . Typical diffuse medium values were added as tickmarks on the right of each panel. The measurements of the  $\lambda 5780$  Å DIB are also shown, for comparison. From Fig. 2, it can be seen that:

- (i) the three DIBs,  $\lambda\lambda 5797$ ,  $6379$  and  $6613$  Å are weakened by a factor 2.5 in the HII Orion region. This confirms the assumption that the carriers can not survive strong UV flux in their state;
- (ii) in the Taurus-Perseus thin cloud an increase of the DIBs strength with increasing reddening can be observed from  $E_{(B-V)} = 0.10$  to 0.3;
- (iii) in the denser parts of the Tau-Per region the DIB strength shows a decrease with reddening.

Such a UV flux dependence in Orion has already been suggested in previous studies for two other DIBs, namely  $\lambda 6196$  Å

**Table 1.** Program star parameter summary: target HD names, star location (Loc),  $E_{(B-V)} \pm 0.02$ , visual magnitude V, spectral type SpT, DIBs equivalent width in mÅ per unit reddening  $W/E_{(B-V)}$  with corresponding error. The location of most stars was defined as following: ORI for Orion stars, TAU for Taurus-Perseus stars, SCO for stars belonging to the Sco-Ophiucus complex and DIFF for the Diffuse medium stars. For each region, stars are ordered according to decreasing  $E_{B-V}$

HD	Loc	$E_{(B-V)}$	V	SpT.	5797 Å	err	6379 Å	err	6613 Å	err	5780 Å	err
183143	DIFF	1.28	6.86	B7Iae	148	8	91	5	253	2	594	14
208501	DIFF	0.76	5.80	B8Ib	109	4	76	8	168	3	279	12
190603	DIFF	0.72	5.64	B1.5Iae	114	11	122	5	146	4	590	16
21389	DIFF	0.54	4.54	A0Iae	107	6	81	6	283	9	713	19
15570	CAS	1.02	8.13	O4	158	9	88	20	249	10	509	13
BD40°4220	CYG	2.00	9.10	O7e	95	10	44	3	153	2	410	10
198478	CYG	0.54	4.84	B3Iae	130	37	185	11	259	6	470	18
206165	CEP	0.47	4.73	B2Ib	151	21	130	29	247	9	358	17
207260	CEP	0.47	4.29	A2Ia	181	12	160	13	309	11	447	16
154445	SCO	0.42	5.64	B1V	100	3	79	12	226	7	505	12
149757	SCO	0.32	2.56	O9.5V	78	3	63	7	109	9	244	6
145502	SCO	0.24	4.01	B2IV	142	42	133	29	217	21	875	35
144217	SCO	0.19	2.62	B0.5V	57	6	74	6	211	16	963	42
30614	CAM	0.32	4.29	O9.5Iae	103	16	109	16	197	10	375	10
184915	AQL	0.30	4.95	B0.5III	77	26	87	10	180	7	547	13
29647	TAU	1.03	8.31	B8III	32	8	14	3	50	2	50	3
283812	TAU	0.71	9.48	A0III	82	10	71	8	159	13	204	10
24534	TAU	0.59	6.10	O9.5ep	83	5	73	4	108	16	56	3
27311	TAU	0.34	8.00	A0	229	30	141	10	232	9	515	13
24912	TAU	0.34	4.04	O7e	91	6	97	9	203	6	535	14
27778	TAU	0.33	6.36	B3V	94	6	61	3	85	6	288	9
23180	TAU	0.30	3.83	B1III	170	7	123	7	157	17	183	6
24398	TAU	0.29	2.85	B1Ib	178	14	197	7	166	10	162	8
22951	TAU	0.24	4.97	B0.5V	125	42	83	21	133	14	188	8
23480	TAU	0.08	4.18	B6IVe	13	3	59	6	38	3	186	9
23302	TAU	0.05	3.70	B6IIIe	40	5	40	6	50	5	260	8
37061	ORI	0.50	6.83	B01V	50	18	60	14	80	30	332	20
37020	ORI	0.40	6.73	O7	48	20	28	12	51	30	75	10
37022	ORI	0.36	5.13	O6	31	14	45	25	45	25	277	25
36861	ORI	0.12	3.66	O8e	161	25	38	4	70	8	317	15
36822	ORI	0.11	4.41	B0III	136	9	100	20	27	11	55	10
37742	ORI	0.09	1.90	O9.5Ibe	19	3	19	11	28	5	100	20
37128	ORI	0.08	1.70	B0Iae	50	2	38	3	38	2	100	7
38771	ORI	0.07	2.06	B0.5Iav	14	7	57	14	29	15	429	14
36486	ORI	0.07	2.23	B0III	42	5	43	14	43	20	129	9

and  $\lambda 6284$  Å (Jenniskens et al. 1994, Ehrenfreund & Jenniskens 1995).

### 3.2. Dehydrogenation versus ionization

Among the most probable gas phase molecular candidates which may show a strong environmental dependence are PAHs or fullerenes. Rotational contour calculations and substructure measurements (Ehrenfreund & Foing 1996) of the observed line profiles of the  $\lambda 6613$  Å DIB led to a PAH size estimation of 40 C atoms.

Recent studies on interstellar PAHs (Jochims et al. 1994, Allain et al. 1996a, b) showed that fully hydrogenated neutral PAHs containing less than 40 C atoms could not survive the ISM Radiation Field (Draine average ISMRF, 1978), in good agreement with size estimations from DIB substructures. Assuming that the DIB strength variations are due to a modification of

the ionization or hydrogenation state of the carrier molecules, defining such processes should help to constrain the nature of the carriers. A study of the hydrogen coverage  $\alpha$ (%) of neutral PAHs and their cations led Allain et al. (1996a) to the conclusions that, independently from the astrophysical environment:

1. PAHs with more than 40 C atoms have the same degree of hydrogenation in the neutral or cationic state;
2. in HI regions (Tau-Per molecular cloud), the hydrogen coverage is around 92% for a 40 C atom PAH and increases linearly to 100% for 50 C atom molecules;
3. the calculated ionization rates are 5 orders of magnitude higher than the hydrogen loss rates ( $10^{-9}$  vs  $10^{-14}$ ,  $10^{-16}$ ) for molecules of more than 40 C atoms.

Consequently, if PAH molecules may account for some DIBs, dehydrogenation does not seem to be a dominant process influencing the DIB behaviour. This confirms that ionization, recom-

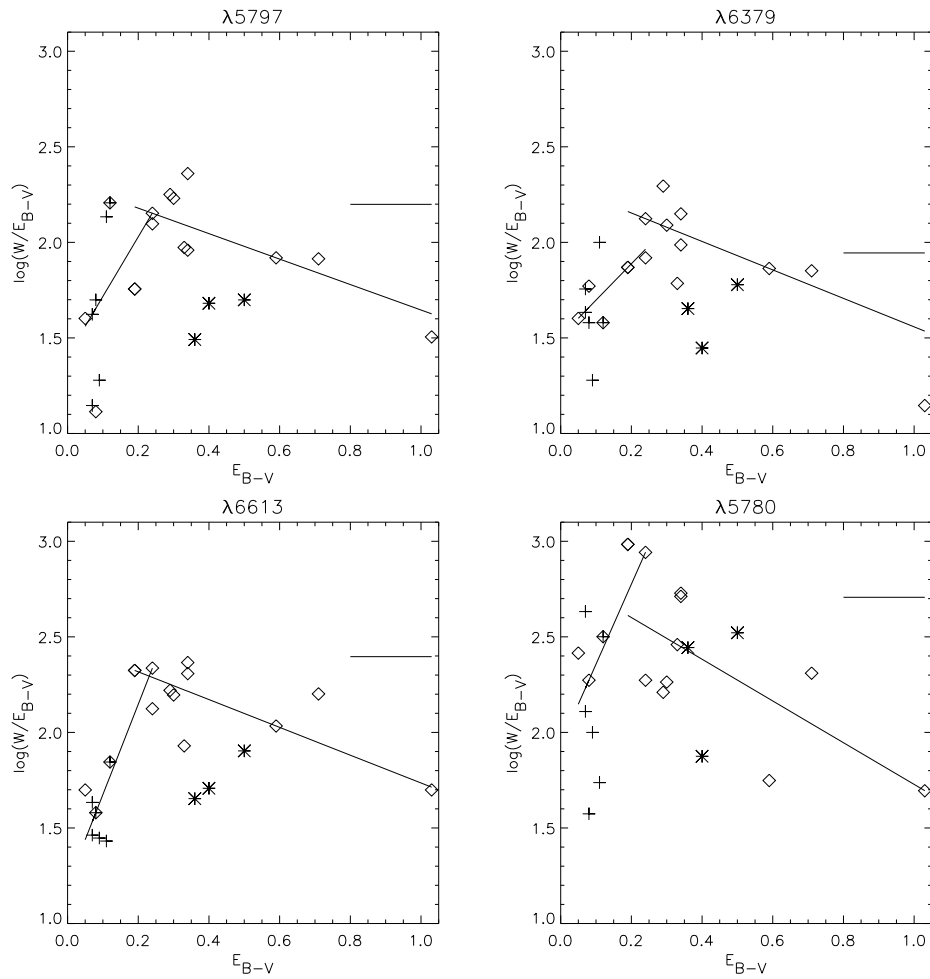


**Fig. 2.** DIB strength decimal logarithm  $\log(W/E_{(B-V)})$  vs  $E_{(B-V)}$  for the four DIBs:  $\lambda 5797$  Å,  $\lambda 6379$  Å,  $\lambda 6613$  Å and  $\lambda 5780$  Å. + denote Orion stars, \* denote Trapezium stars,  $\diamond$  are Taurus-Perseus targets, the diffuse medium DIB intensities are represented by the solid line on the right of each panel.

bination and destruction are the dominant processes responsible for the environmental behaviour of the DIBs.

Recent laboratory work on PAHs (Salama et al. 1996), as well as theoretical calculations, indicate that the interstellar distribution of small compact PAHs is limited to only two charge states, namely neutrals (0) and cations (+1). For larger species, three or more charge states are possible and anions (-1) become dominant at high electron densities. Therefore, being able to estimate the abundance ratios for one charge state to the next state  $(n+1)/(n)$  and  $(n-1)/(n)$  of a given molecule may, by comparison with observations, give some clues for the identification puzzle.

### 3.3. The ionization equilibrium model

For a gas phase molecule M in a charge state (n), assumed to be the carrier of a diffuse band, the abundance yields are defined by Eqs. (1) and (2) as follows:

$$\frac{M^{n+1}}{M^n} = \frac{K_{ion}\Phi_{n,n+1}}{K_{rec}N_e} \quad (1)$$

and

$$\frac{M^{n-1}}{M^n} = \frac{K_{rec}N_e}{K_{ea}\Phi_{n-1,n}}$$

where  $K_{ion}$ ,  $K_{rec}$ ,  $K_{ea}$  are the ionization, recombination and electron attachment coefficients, respectively.  $N_e$  is the electron density and  $\Phi_{n,n+1}$ ,  $\Phi_{n-1,n}$  the flux number of photons with energy  $E^+$  and  $E^-$ , sufficient to go from a charge state (n) to (n+1) and from a charge state (n-1) to (n). Eqs (1) and (2) indicate a variation of the molecule abundance ratios with the radiation intensity and the electron density. According to Allain et al. (1996), the electron density varies 100 times less than the flux in our regions of interest (the Orion PDR and the Taurus HI region). We therefore assumed the abundance variations to follow the UV flux variations only, neglecting the density effects. We can distinguish two domains where  $M^{n-1} \ll M^n \ll M^{n+1}$  and  $M^{n-1} \gg M^n \gg M^{n+1}$ .

In the conditions of thin clouds where UV penetrates and

$$\frac{M^{n+1}}{M^n} \gg 1$$

all over the cloud, the carrier density  $M^n$  is proportional to  $(\Phi_{n,n+1})^{-1}$ . To estimate  $\Phi$ , we considered a cubic cloud of optical thickness  $\tau_c$  at its center. The UV flux along a line-of-sight passing through the center of the cloud and crossing the center of two of the cube's sides can, hence, be approximated by

$$\Phi \approx \Phi_0 \left[ \frac{2}{3} e^{-\frac{\tau_c}{2}} + \frac{1}{6} (e^{-\tau} + e^{\tau - \tau_c}) \right] \quad (3)$$

The second part of Eq.(3) contains two terms. The first term represents the flux contribution to the line-of-sight, from the 4 sides of the cubic cloud which are not crossed by the line-of-sight. The second term represents the flux contribution from the 2 planes crossed by the line-of-sight passing through the center of the cloud.  $\Phi_0$  is the total IRF the cloud bathes in. The molecule abundance in the charge state  $M^n$  peaks in the center of the cloud where the UV flux is about  $\Phi_0 e^{-\frac{\tau_c}{2}}$ . The DIB equivalent width (W), proportional to the integrated M column density through the cloud, varies in general as

$$W \approx \int M \approx \int \frac{1}{\Phi} d\tau = 3e^{\frac{\tau_c}{2}} \int_{-\frac{\tau_c}{2}}^{\frac{\tau_c}{2}} \frac{dx}{2 + chx} = f(\tau_c) \quad (4)$$

We calculated that  $f(\tau_c)$  changes as  $\tau_c 10^{\frac{\tau_c \beta}{5}}$  where the correction factor  $\beta$  varies slightly from 2 asymptotic values of 1.1 for  $0 < \tau_c < 1.5$  to 0.84 for  $\tau_c > 3.0$ . We used an average normalized extinction curve to estimate the UV flux at a given wavelength as follows:

$$\Phi_{n,n+1} = \int_{E>IP} \Phi_{UV} dE \quad (5)$$

with

$$\Phi_{UV} \approx \Phi_{UV}^o 10^{-\frac{A_\lambda}{E_{B-V}} \frac{E_{B-V}}{2.5} \frac{1}{2\alpha}} \quad (6)$$

where  $\Phi_{UV}^o$  is the UV field outside the clouds and  $\Phi_{UV}$  is the UV field seen after absorption by the cloud shell.  $\lambda$  is taken at the energy of the ionization potential,  $\alpha \approx 1$  is a geometrical factor for the shape of the cloud. For a given effective  $\lambda$  the quantity

$$\frac{A_\lambda}{E_{B-V}} = A'_\lambda + R_V \quad (7)$$

can be obtained from the extinction curves.  $A'_\lambda$  represents the extinction curve normalized to 0 at V and 1 at B.

By combining Eqs. (1), (4) and (6), this model predicts for a given DIB that  $\log(W/E_{B-V})$  varies almost linearly with  $E_{B-V}$  as:

$$\frac{A_\lambda}{E_{B-V}} \frac{\beta}{5\alpha} E_{B-V} - \log \frac{N_e K_{rec}}{K_i \Phi_0} + \log \frac{\tau_c}{E_{B-V}} + Cte \quad (8)$$

The ‘‘slope’’ of this relation is used in the next section to estimate the ionization potential of the DIB carriers.

In the conditions at high  $E_{B-V}$  where

$$\frac{M^n}{M^{n-1}} \ll 1$$

in most of the cloud,  $M^n$  varies as  $\Phi_{n-1,n}$  and is abundant only in the outer layer of the cloud. The integrated column density of M reaches a limit above  $\tau_c = 9$  which carries no further information on  $\tau_c$  but leads to a ‘‘ $\log(W/E_{B-V})$  slope’’ of (-1) for high reddening.

**Table 2.** Calculated slopes for different photon energies using the wavenumber  $\lambda^{-1}$  and its corresponding  $A'_\lambda$  derived from an average normalized extinction curve as well as typical Orion and Taurus  $R_v$  values of 3.0, 3.6 and 5.1 respectively.  $\tau_c$  is the corresponding optical thickness for  $E_{B-V} = 0.10$ .

E(eV)	$\lambda^{-1}(\mu^{-1})$	$A'_\lambda$	$R_v=3.0$	3.6	5.1	$\tau_c$
4.0	3.22	2.50	1.10	1.22	1.52	1.40
6.5	5.20	5.50	1.70	1.82	2.12	1.95
8.0	6.45	6.00	1.80	1.92	2.22	2.04
10.0	8.00	8.50	2.30	2.42	2.72	2.50
12.5	10.00	16.00	3.80	3.92	4.22	3.90
13.0	10.40	17.50	4.10	4.22	4.52	4.16

**Table 3.** Observed slopes for the three DIBs  $\lambda\lambda 5797, 6379$  and  $6613 \text{ \AA}$  with their respective deviations. The  $\lambda 5780 \text{ \AA}$  DIB was added for comparison.

Region	$\lambda 5797 \text{ \AA}$	$\lambda 6379 \text{ \AA}$	$\lambda 6613 \text{ \AA}$	$\lambda 5780 \text{ \AA}$
Positive slopes	3.12	1.90	4.72	4.19
Deviation	0.26	0.13	0.12	0.28
Negative slopes	-0.67	-0.74	-0.73	-1.09
Deviation	0.17	0.17	0.15	0.32

#### 3.4. Ionization potential and DIB variation vs reddening

In the frame of the ionization model we can predict ‘‘slopes’’ as follows:

$$\frac{A_\lambda}{E_{B-V}} \frac{\beta}{5\alpha}$$

that can be calculated using extinction curves (Savage et al. 1977). We considered ionization potential values ranging from 4 to 13 eV and calculated the slopes with the above equations and typical Taurus and Orion  $R_V$  values of 3.0, 3.6 and 5.1. This led us to an  $A'_\lambda$  estimation ranging from 2.5 to 17.5 with a typical error of 0.10. We summarized the slope values of the expected linear behaviour in Table 2. Considering the ionization equilibrium model assumptions, the UV flux is the determining parameter in the charge state variations of the species. A linear fit of the data should consequently give us slopes, and hence, estimations of the charge state yields to be compared with the calculated results. Therefore, the observation of lines-of-sight with different average UV field penetrations should mimic this charge state evolution.

#### 3.5. Comparison with observations

Fig. 2 shows the decimal logarithm of the normalized equivalent width  $W/E_{B-V}$  versus reddening for the Taurus and Orion stars observed in the survey. Consistently with ionization equilibrium we see a rise and fall of the DIB strength. In order to derive the slopes on the HII and HI regions of the program stars, we applied a least absolute deviation method on the following samples:

(i) The positive slope was obtained considering the two ‘‘Pleiades’’ stars HD23480 and HD23302, where the DIBs are strongly weakened, the two Sco-Oph stars HD145502 and HD144217, in addition to the Orion stars HD37742, HD37128,

HD36861, HD38771, HD36 486 and HD36822.

(ii) As the physical conditions in the Orion Trapezium stars region are not yet well defined, the errors on the measurements of these three stars (HD37020-22 and HD37061) can be as large as 50%. We, therefore, did not include them for the determination of the slopes. We also find that those measurements are significantly below data for other lines-of-sight, showing the strong and hard UV radiation conditions in regions near hot bright stars.

(iii) The negative slope was derived using the Tau-Per stars and the two former Sco-Oph stars HD144217 and HD145502. These two stars were added to both samples in order to better represent the edge conditions of molecular clouds ( $E_{B-V} \approx 0.19-0.25$ ). Data slope estimates and uncertainties are given in Table 3 for the four DIBs.

The comparison between the calculated and data derived slopes led us to several conclusions. Within the error bars, the negative slopes for  $\lambda\lambda 5797, 6379$  and  $6613 \text{ \AA}$  are equal to  $-0.70$ . This means that these three DIB carriers do behave the same way with respect to molecular cloud conditions where they may be converted into the next lower ionization state.

The positive slopes for the  $\lambda\lambda 5780, 5797$  and  $6613 \text{ \AA}$  DIBs ranging from 3.12 to 4.72 lead to an ionization potential energy range of 10.0 to 13.5 eV, after extrapolating our average normalized extinction curve.

In the PAH frame, these energies are compatible with second ionization energies suggesting the carriers of these three bands could be already single PAH cations.

On the other hand, the  $\lambda 6379 \text{ \AA}$  has a positive slope of 1.90, smaller than the other DIB slopes. We can derive for  $\lambda 6379 \text{ \AA}$  an ionization potential energy range of 7–9 eV compatible with first ionization potential of neutral PAHs. The limiting factor is the dispersion of the extinction curves of different lines-of-sight, in the sample (see Eqs. (6) and (8)).

Finally, the slope intersections (where the carrier abundance peaks) for  $\lambda\lambda 6613, 5797$  and  $6379 \text{ \AA}$  occur at  $E_{B-V}$  equal to 0.23, 0.25 and 0.30, respectively, with a typical error of 0.03 (see Fig. 2). The  $\lambda 5780 \text{ \AA}$  slope intersection occurs at  $0.17 \pm 0.03$ , which means that the  $\lambda 5780 \text{ \AA}$  carrier molecule reaches its maximum for higher UV photon energy values than the three other DIBs. This confirms the assumption that the  $\lambda 5780 \text{ \AA}$  carrier is favoured and more resistant in strong UV flux conditions. Thus, the position of the slope intersection seems to reflect the order of the ionization potential of the carriers.

### 3.6. Sources of errors and limits of the model

The discrepancies between the calculated and observed slopes can have various origins. First of all, we neglected the gradient of electronic density times recombination rates compared to the gradient of UV photoionization. Recent work on molecular clouds shows that molecular clouds and PDR are clumpy (Spaans 1996). This can have two effects on the results.

1. the UV field in a PDR can significantly fluctuate from one line-of-sight to another leading to abnormal DIB strengths

because of UV penetration variations. The resulting “slope” is hence a superposition of various “slopes”.

2. the modification of  $N_e$  implies a modification of the charge state yields (see Eqs. (1) and (2)) and hence a change in the slope, lower in Orion and increased in Taurus.

A flux integration over the whole line-of-sight, taking into account the medium geometry and extinction cross-section should be performed to improve this estimation. We assumed a cloud geometry factor  $\alpha$  of 1, in the frame of an approximation of UV penetration in a cubic cloud.

To compare different lines-of-sight, we assumed the same ISMRF (Draine 1978), but there could be variations from cloud to cloud. Some of the dispersion in the value of  $\log(W/E_{B-V})$  can arise, as predicted, from our model, from the extinction curve differences in the various lines-of-sight of the sample.

The measurement inaccuracies from the reduction method could introduce some systematic errors, especially when normalizing to unit reddening. Finally, we pointed out specific carriers, namely PAHs, but the slopes and derived ionization potentials could also be consistent with neutral or ionized fullerenes, which have similar ionization potentials. Furthermore, profile substructures are also compatible with 12-18 C-chains and 30 C-rings (Ehrenfreund & Foing 1996) or 14-30 C-rings (Kerr et al. 1997).

## 4. Conclusions

The survey of 40 lines-of-sight constituted of 35 program stars and 5 standard stars, in regions representing different physical properties like UV field intensities and density confirmed that the band strength of the  $\lambda\lambda 5797, 6379$  and  $6613 \text{ \AA}$  DIBs is directly linked to the variation of these parameters.

We developed a simple photoionization equilibrium model linking the carrier molecule abundances, via the measured DIB strength, with the UV flux penetration inside the cloud (at the ionization potential energy). The results show that, assuming PAH carriers, the DIB carrier charge state yields could be reasonably reproduced using the measured normalized equivalent width. This method led us to the conclusion that the  $\lambda\lambda 5797, 6379$  and  $6613 \text{ \AA}$  DIBs are due to three different gas phase molecules. Our results indicate that the three DIB carriers have a similar behaviour in regions of low UV flux penetration, like the Taurus HI region. On the other hand, they show a rather different behaviour (in terms of destruction efficiency) in Photon-Dominated-Regions like the Orion HII region, pointing out different ionization potentials.

They are, however, related for the following reasons:

1. the three narrow DIBs are the first for which substructures have been resolved indicating large gas phase molecules. Rotational contour modelling of the peak separation indicates possible sizes of 40 and 50 C atoms (if PAHs) for  $\lambda\lambda 6613, 5797$  and  $6379 \text{ \AA}$ , respectively.
2. these DIBs are enhanced in the dense line-of-sight towards BD +63° 1964 compared to HD183143 with a relative ratio of 1.22, 1.72 and 2.12 varying inversely with the ionization potential (Ehrenfreund et al. 1997).

3. the  $\lambda 6613$  DIB increases at low reddening 1.5 times faster than the  $\lambda 5797$  DIB, indicating slightly higher ionization potential (respectively 13 eV and 11 eV within our modelling assumptions). These values are consistent with single cation ionization potentials, considering PAH carriers.
4. the  $\lambda 6379$  Å DIB seems to be due to a carrier molecule with ionization energy between 7 and 9 eV, as expected for a large neutral molecule.
5. the  $\lambda\lambda 5797$  and  $6613$  Å DIBs reach their maximum at the same  $E_{B-V}$ , within the error bars, but at harder UV than the  $\lambda 6379$  Å.
6. the  $\lambda 5780$  Å DIB reaches its maximum at lower  $E_{B-V}$  than the three other DIBs indicating that this cation molecule is more resistant to strong UV fields than the  $\lambda\lambda 5797$ ,  $6379$  and  $6613$  Å carriers.

These results seem to confirm the correlation study of Cami et al. (1997) who concluded these three DIBs likely belong to an isolated carrier family. The approach we have followed is in principle a new and interesting quantitative tool to characterize the ionization properties of other DIB carriers than the three presented here. This will require high precision observations of selected lines-of-sight offering a comprehensive sequence of ultraviolet flux penetration.

A refinement of the model with a better UV extinction estimate as well as the inclusion of electronic recombination, hydrogenation and three dimensional radiative transfer effects should be carried out when relevant astronomical measurements are available. There is a strong need for determination of corresponding ionization potentials and rates of candidate carrier molecules from laboratory measurements. Line profile observations and modelling which lead to estimates of the molecular size and rotational temperature will complement the information on ionization properties and lead to the identification of the DIB carriers.

*Acknowledgements.* We thank M. Spaans for helpful comments. P. Sonnentrucker acknowledges MESR (Ministère de l'Enseignement Supérieur et de la Recherche, France) for a doctoral fellowship ( $n^{\circ}96067$ ). We thank the staff of OHP for help during the observations. We also thank Leiden University and the Solar System Division

at ESTEC/ESA for financial and computing facilities support. P. Ehrenfreund is a recipient of an APART fellowship of the Austrian Academy of Sciences.

## References

- Adamson A., Whittet D.C.B., Duley W.W., 1991, MNRAS 252, 234A  
 Allain T., Leach S., Sedlmayr E., 1996a, A&A 305, 602  
 Allain T., Leach S., Sedlmayr E., 1996b, A&A 305, 616  
 Cami J., Sonnentrucker P., Ehrenfreund P., Foing B.H., 1997, A&A in press  
 Draine B.T., 1978, ApJS 36, 595  
 Ehrenfreund P., Jenniskens P. 1995, in Diffuse Interstellar Bands, eds. Tielens A.G.G.M. & Snow T., Kluwer Academic Publisher, 105  
 Ehrenfreund P., Foing B.H. 1995, CCP7/PCMI Newsletter 22, 18  
 Ehrenfreund P., Foing B.H. 1996, A&A 307, L25  
 Ehrenfreund P., Cami J., Dartois E., Foing B.H. 1997, A&A 318, L28  
 Foing B.H., Ehrenfreund P., 1994, Nature 369, 296  
 Foing B.H., Ehrenfreund P., 1997, A&A 317, L59  
 Herbig G.H., 1993, ApJ 407, 142  
 Herbig G.H., 1995, Annual Review A&A 33  
 Jenniskens P., Ehrenfreund P., Foing B.H., 1994, A&A 281, 517  
 Jochims H.W., Ruhl E., Baumgartel H., Tobita S. and Leach S., 1994, ApJ 420, 307  
 Kerr T.H., Hibbins R.E., Miles J.R., Fossey S.J., Somerville W.B. and Sarre P.J., 1996, MNRAS 283, L105  
 Krelowski J., Walker G.A.H., 1987, ApJ 312, 860  
 Krelowski J., Megier A., Strobel A., 1996, A&A 308, 908  
 Krelowski J., Schmidt M., 1997, ApJ 477, 209  
 Salama F., Bakes E.L.O., Allamandola L.J., Tielens A.G.G.M., 1996, ApJ 458, 621  
 Sarre P.J., Miles J.R., Kerr T.H., Hibbins R.E., Fossey S.J., Somerville W.B., 1995, MNRAS 277, L41  
 Savage B.D., Bohlin R.C., Drake J.F. and Budich W., 1977, ApJ 216, 291  
 Snow T.P., JR., Cohen J.G. 1974, ApJ 194, 313  
 Snow T.P., Bakes E.L.O., Buss R.H., Seab C.G., 1995, A&A 296, L37  
 Spaans M. 1996, A&A 307, 271

This article was processed by the author using Springer-Verlag L<sup>A</sup>T<sub>E</sub>X A&A style file L-AA version 3.